Optical fiber Bragg grating (FBG)-based strain sensor embedded in different 3D-printed materials: A comparison of performance

Mohamad Ashraff Alias [a], Harith Ahmad [a,b,c,d,*], Muhammad Khairol Annuar Zaini [a], Muhamad Zharif Samion [a], Muhammad Syamil Mohd Sa'ad [a], Lim Kok Sing [a], Kenneth T.V. Grattan [e], B.M. Azizur Rahman [e], Gilberto Brambilla [f], Siti Aisyah Reduan [a], Leonard Bayang [a], Mohammad Faizal Ismail [a]

[a] *Photonics Research Center, Universiti Malaya, 50603 Kuala Lumpur, Malaysia*
[b] *Department of Physics, Faculty of Science, Universiti Malaya, 50603 Kuala Lumpur, Malaysia*
[c] *Universiti Kuala Lumpur British Malaysian Institute (UniKL BMI), Batu 8, Jln Sungai Pusu, 53100 Selangor, Malaysia*
[d] *Department of Physics, Faculty of Mathematics and Natural Sciences, Universitas Negeri Malang, Jalan Semarang 5, Malang 65145, Indonesia*
[e] *School of Mathematics, Computer Science & Engineering, University of London, London EC1V 0HB, United Kingdom*
[f] *Optoelectronics Research Center, University of Southampton, Southampton SO17 1BJ, United Kingdom*

Abstract

A compact and inexpensive fiber Bragg grating (FBG)-based strain sensor has been developed by embedding an FBG inside a 3D-printed structure, allowing the comparison of FBG responses across different filaments such as polylactic acid (PLA), thermoplastic polyurethane (TPU), polycarbonate (PC), acrylonitrile butadiene styrene (ABS), and nylon. Results have shown that FBG embedded in TPU can be applied effectively in the measurements of mechanical strain, giving a responsivity value of 17.70 pm/cm of displacement with outstanding linearity (98%). Furthermore, small-scale field testing conducted in below-ground environments has shown that strain sensors based on FBG embedded in TPU are the most effective. They offer a responsivity of 13.9 pm/kg with a small standard deviation and high linearity. Additionally, they also give a temperature sensitivity value of 15.4 pm/°C, which was the highest compared to the other embedded FBGs. Therefore, for most industrial applications, FBG embedded in TPU can be considered as an alternative to existing embedment methods for strain sensing applications.

Keywords: Fiber Bragg grating, Strain sensor, 3D printing technology, Thermoplastic Polyurethane, Polylactic Acid, Polycarbonate, Acrylonitrile Butadiene Styrene, Nylon.

1. Introduction

The advances made in laser systems and modern low-loss optical fiber in the 1960s had become the primary catalyst to the meteoric progression of optical fiber sensing technology in this contemporary era [1]. The propensity of such advancement in transmitting a vast amount of data compared to other electrical and microwave systems has encouraged researchers to

evaluate the possibility of optical fibers for data communication and various applications in the sensing field [2]. During the 1970s, the development of optical fibers has been growing rapidly through some pioneering work on low-loss optical fiber where a silica-core multi-mode optical fiber with losses of about 0.2 dB/km was achieved [2]. This, in return, had significantly broadened the possible applications of optical fiber sensors through the combination of optoelectronic devices and optical fiber communications. Aligning with the continuous improvement and demand of these devices by some related industries, the cost of such components has also decreased, allowing this optical-based sensing technology to compete with existing conventional technologies in various applications.

In contemporary times, the implementation of optical fiber sensors is seen to be an exemplary solution for many field applications that require constant monitoring due to the favourable attributes that it possesses, such as outstanding geometric versatility [3,4]. Furthermore, as no electrical currents are flowing through sensing element, they are also known to be free from any external electromagnetic field interference (EMI) [4–7]. Apart from that, sensors of this type are also compact [7], equipped with excellent mechanical flexibility [7], [8] and offer better sensitivity compared to existing electrical-based sensors [9], as well as providing ease of installation [10]. Fiber Bragg gratings (FBG) are perceived to be one of the most typical kinds of optical sensors as they have all these traits. FBG-based sensors can also be applied in numerous industrial applications due to their tremendous adaptability in harsh environments [8,11], thus making them one of the essential alternatives in the field of electrical, civil, mechanical, medical, automotive, nuclear, and aerospace sensing [12]. Moreover, they also provide a high possibility of cost-effectiveness based on their multiplexing ability, reduced fiber usage, installation, instrumentation, and maintenance costs [12]. They also provide quasi-distributed monitoring compatibility [13] and excellent chemical stability [13]. Being point sensors, they can also be applied to compute several physical parameters such as temperature, strain, displacement, vibration, tilt angles, and viscosity [14–16].

Using FBG will be an interesting option for strain sensors as it gives many distinct advantages, as mentioned earlier. For example, Chen *et al.* [17] developed an FBG-based strain sensor by directly embedding the FBG inside a glass fibre-reinforced plastic (GFRP) to monitor the GFRP's strain changes under loading. Despite being strong, lightweight, and corrosion resistant, the sensor produced convoluted responses due to inconsistency of the GFRP's layer thickness. On the other hand, Tanaka *et al.* [18] have administered a dissimilar approach where two serially connected FBGs are embedded in composite laminates, which incorporates the use of both CFRP and glass fibre-reinforced plastic (GFRP), which was intended for temperature-

compensated strain sensing. Due to the difference in coefficient of thermal expansion (CTE) between CFRP and GFRP, any temperature changes that exist in this sensor can be compensated. However, this method requires a complex and detailed preparation method, which will not be cost-effective in large-scale manufacturing. The above techniques are also time-consuming as they would need different molds and a specific instrument in their fabrication process. Apart from that, these methods had also shown lesser performance repeatability of their sensors.

The direct attachment of an FBG to a structure under investigation using a protective coating such as epoxy has also been reported in some works [19,20]. For instance, Mao *et al.* [20] used this approach in developing a strain sensor intended for corrosion monitoring of reinforced concrete structures. An FBG was securely attached to a concrete structure using epoxy. As corrosion occurs, this will cause the concrete to expand, and then cause the FBG sensor to bend. This bending induces strain on the FBG, resulting in wavelength shifts in the output spectrum. These shifts provide a direct measure of the applied strain, offering insights into corrosion activity and its effects on structural integrity. However, this method has its limitations. Firstly, the use of epoxy for fixing FBGs to structures prolongs the preparation time, as the epoxy requires a curing period of at least 12 to 24 hours for light usage and up to 7 days for heavy usage. Furthermore, for applications demanding higher sensitivities, such as landslide monitoring, directly affixing a bare FBG to a structure (particularly an inclinometer or extensometer) may prove impractical, as the optical fiber remains exposed to harsh conditions and is prone to breakage due to its fragile nature unless additional protective measures are implemented. Additionally, the use of epoxy can hinder the stretching of the FBG, resulting in reduced strain and may alter the measurements at the point of analysis. Thus, directly fixing an FBG to a structure under investigation may not be suitable for applications exposed to harsh environments, particularly those involving the detection of ground movements. Table 1 presents the comparison between existing works and our work based on the materials used to embed the FBG, measured parameters, desired application, as well as the advantages and disadvantages of each sensor.

1

2

3

Table 1. Comparison of FBG-based strain sensors between existing works and our work

Ref.	Materials Used to Embed the FBG	Measured Parameters	Desired Application	Advantages	Disadvantages
[17]	Glass Fiber-Reinforced Plastic (GFRP)	• Circumferential strain • Axial strain	Monitoring of composite tube structures	• Can measure both circumferential and axial strain	• The spectrum of the FBG has a dual-spike signal • Tested only in laboratory environment
[18]	• Carbon Fiber-Reinforced Plastic (CFRP) • Glass Fiber-Reinforced Plastic (GFRP)	• Strain • Temperature	Temperature-compensated application	• Accurate strain measurement • Temperature-compensated measurement	• Complex manufacturing process • Tested only in laboratory environment
[20]	Epoxy Resin	• Crack width • Concrete expansion	Monitoring of corrosion process in reinforced concrete structures	• Can monitor concrete cracking • Can monitor corrosion process	• Fragile sensor design • Tested only in laboratory environment
This work	• PLA • TPU • PC • ABS • Nylon	• Horizontal displacement • Temperature	Applications that require high sensitivities such as monitoring of landslides	• Ease of fabrication • Flexible sensor • Repeatable measurement • Tested in a small-scale field test	• More testing needed in real application

In order to overcome such limitations, 3D printing technology can play a vital role in the manufacturing process. As it is also known as additive manufacturing, this technology has been gathering interest from researchers and manufacturers throughout the globe due to its fast manufacturing process, cost-effectiveness, wide availability of available materials, ease of

fabrication, and also serve as an eco-friendly solution to a variety of applications [19–22]. As optical-based sensors have compatibility with a variety of polymers [23–25], 3D printing technology can be helpful in fabricating the sensor body for FBGs, thus enabling it to perform effectively upon bending.

Previous work by Hong *et al.* [26] demonstrated the implementation of 3D printing technology to fabricate an FBG-based pressure sensor where a PLA material was used to embed the FBG for the evaluation of vertical pressure. In this work, a sensitivity of 13.22 pm/kPa was attained with a maximum measurement range of 2000 kPa. Furthermore, Ismail *et al.* [27] also demonstrated the same approach where a temperature-independent FBG-based tilt sensor, which comprises 5 FBGs (4 for tilt measurement and 1 for temperature compensation), was developed by fabricating the sensor body using a PLA material for the measurement of tilt angles in 4 directions (+x, -x, +y, and -y). Based on the conducted tests, an average FBG response of 0.01nm/degree of tilt was obtained by all 4 strain-sensitive FBGs over the range of 0° to 90°. Another work by Alias *et al.* [28] also showed the use of 3D printing technology where a temperature-independent FBG-based torsion sensor was developed by embedding an FBG inside a TPU material for the measurements of torsion. In this work, the FBG torsion sensor gives a responsivity of 0.95 pm/degree of rotation over the range of 0° to 100° for both clockwise and counter-clockwise rotation.

Based on the reported works mentioned above, we have decided to use 3D printing technology to fabricate the sensor body of our strain sensor due to its various benefit. Our work focuses on a simple and compact design of an FBG-based strain sensor, specifically highlighting the embedding of 5 FBGs into 5 different 3D-printed materials to compare their mechanical strain and temperature sensing performance. This was done by evaluating the wavelength shifts obtained by each FBG, which is strain-sensitive. The materials used are polylactic acid (PLA), thermoplastic polyurethane (TPU), polycarbonate (PC), acrylonitrile butadiene styrene (ABS), and nylon. The response of all 5 FBGs were also tested in a small-scale field test. An additional 5 FBG, which was strain-insensitive (positioned loosely to only measure temperature), was added to provide temperature compensation during the measurement. In addition to the advantages that FBG-based sensors possess, such as the ability to be multiplexed and lightweight, this FBG-based strain sensor was also characterized by its ease of fabrication and measurement sensitivities based on both sensing requirements and material properties.

2. Sensor structure and its principle

2.1. Strain sensor design and dimensions

The design and dimensions of the proposed FBG-based strain sensor presented in this work are illustrated in Fig. 1 (a), which shows the 3D view, while the cross-sectional top view of the embedded FBG-based strain sensor is shown in Fig. 1 (b).

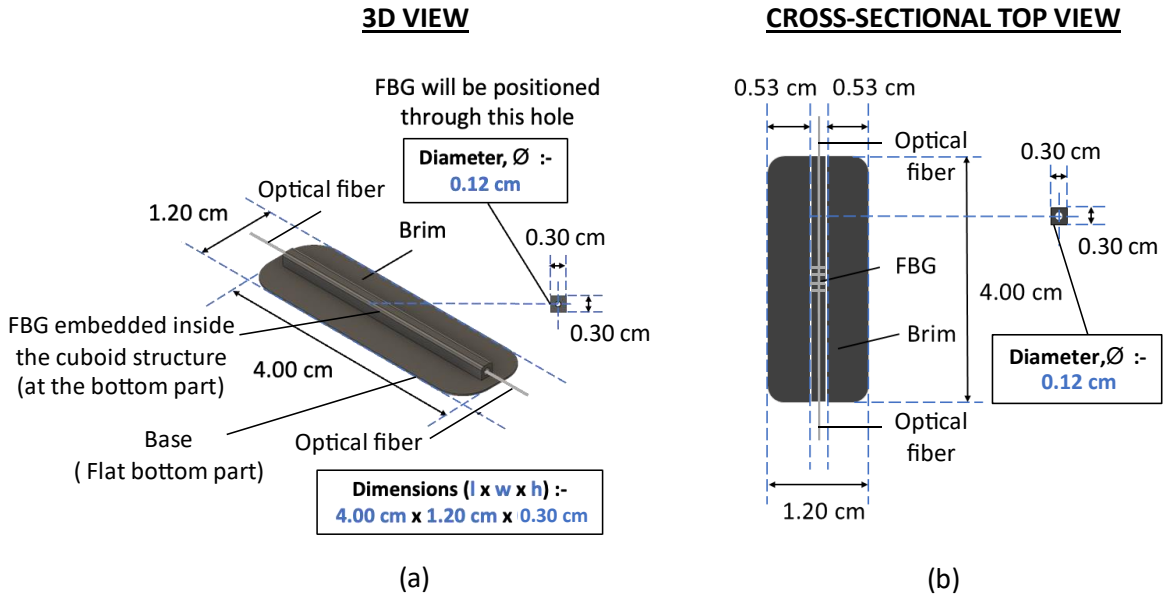

Fig. 1 Illustration of the sensor design, showing the (a) 3D view and (b) cross-sectional top view of the embedded FBG-based strain sensor with dimensions.

In this strain sensor design, the FBG, which acts as the sensing element, was embedded at the bottom part of the 3D-printed cuboid structure with a dimension of 4.00 cm x 1.20 cm x 0.30 cm. Moreover, the dimensions of the cuboid structure only allow stretching along the horizontal axis and bend when vertical forces are applied. As a result, the embedded FBG will solely experience stretching in response to horizontal or vertical bending of the cuboid structure. This limited stretching behavior facilitates easier control of the FBG's response, as it is confined to four directions (+x, -x, +y, and -y). One of the main motivations for this sensor design is to protect the FBG inside the 3D-printed cuboid structure. Since the length of the cuboid structure was set to be 4 cm in length, it will provide enough protection to the FBG in this work, which has a length of 1 cm only. Therefore, extending the length of the cuboid structure would be unnecessary, as it would only result in additional material usage and fabrication time. The 3D printer used in this work was Ultimaker 2+, a fused deposition modeling (FDM)-based 3D printer manufactured by Ultimaker. An FDM-based 3D printer

functions by melting polymers in filament form and stacking them layer by layer according to the path defined by the G-code until an end product is accomplished [19].

Fig. 2 shows the full fabrication process of the FBG-based strain sensor. Firstly, the G-code of the sensor body was uploaded to the 3D printer. Then, the 3D printer prints the sensor body according to the G-code-defined path. Upon printing the sensor body made of PC material, a fiber containing the FBG was fixed inside the cuboid structure. In this procedure, the FBG was first inserted through the hole (Ø = 1.2 mm) of the cuboid structure and was then pre-stressed by pulling each end of the fiber containing the FBG. Each end of the fiber was taped to prevent any movement of the fiber during the gluing process, which was accomplished by applying a portion of cyanoacrylate glue, also known as super glue, to fill up the ring of the holes. After 5 minutes, this was tested to ensure that the fiber is held tightly through the holes of the 3D-printed cuboid structure. The same steps were repeated for materials made of PLA, TPU, ABS and nylon, where the properties and main print settings of each material are presented in Table 2.

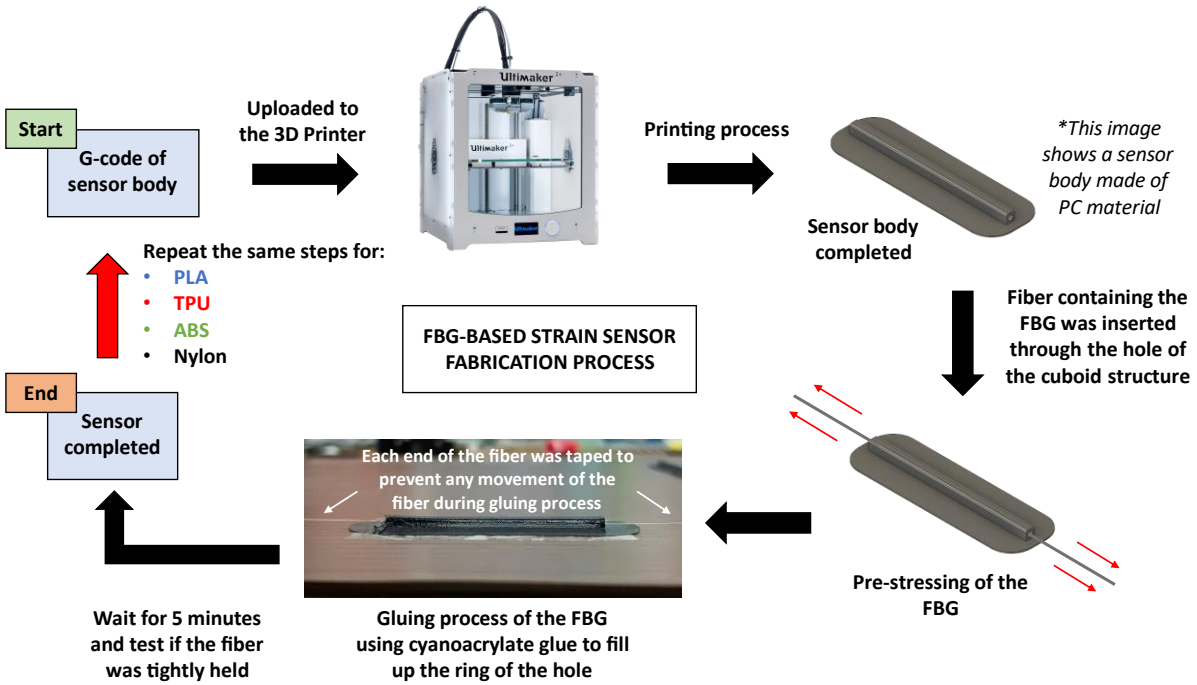

Fig. 2 Illustration of the fabrication process of the FBG-based strain sensor

Table 2. Materials used to embed the FBGs including their properties and main print settings

Ref.	Material	Young's Modulus (GPa)	Coefficient of Thermal Expansion (10^{-6}/°C)	Main Print Settings
[29,30]	PLA	1.80	68.00	• Printing Speed: 60 mm/s • Nozzle Temperature: 220°C • Infill Density: 20% Infill Pattern: Concentric
[30,31]	TPU	0.03	100.00	• Printing Speed: 40 mm/s • Nozzle Temperature: 230°C • Infill Density: 20% Infill Pattern: Concentric
[30,32]	PC	2.00	69.00	• Printing Speed: 50 mm/s • Nozzle Temperature: 270°C • Infill Density: 20% • Infill Pattern: Concentric
[30,33]	ABS	2.90	90.00	• Printing Speed: 50 mm/s • Nozzle Temperature: 260°C • Infill Density: 20% • Infill Pattern: Concentric
[30,34]	Nylon	2.20	95.00	• Printing Speed: 60 mm/s • Nozzle Temperature: 270°C • Infill Density: 20% • Infill Pattern: Concentric

Referring to Table 2, the infill density of all 5 FBG-based strain sensors was set to be at 20% with an infill pattern of the concentric type. A low infill density was chosen on account of the material's stiffness. As the stiffness of a specific material increases, the flexibility that it gains decreases, which will then result in a lower strain sensitivity due to the material being

less stretchable [28]. Furthermore, the performance of the end product of a 3D-printed structure will also be influenced by its infill pattern. Therefore, to establish a compact strain sensor intended for strain measurement, a concentric infill was used as it can provide better strength, flexibility, and time of preparation [4,7,28]. It is because the internal structure of this infill pattern is composed of concentric lines that match the design of the sensor's structure, which, in return, will provide additional strength in both the x and y direction for the sensor design. Fig. 3 shows the layer view of the printed structure, showing the concentric pattern with 20% infill density used in this work. The addition of a brim will enable a larger area of contact and adhesion between the sensor and the outer wall of the PVC pipe. On the other hand, base thickness could also affect how well the sensor is attached to the PVC pipe. A thin base thickness would be preferred because it can be easily stuck at the curvature of the pipe using a double-sided tape. A thicker base will find difficulties to be fitted on the outer walls of the pipe. In addition, a thin base thickness also provides an ease of fabrication for FDM 3D printers enabling good quality prints. For a PVC pipe that is 17mm in diameter, which was used in this work, a 1mm base thickness was considered to be sufficient, offering a combination of enhanced adhesion, improved support, and dimensional stability. It will also enable the FBG embedded at the bottom part of the cuboid structure to perform well as it is in contact with the whole underpart of the sensor body. Moreover, the body of all 5 FBG-based strain sensors was also fabricated similarly in terms of their vertical resolution, which was set at 0.10 mm in Cura slicing software. This was done to ensure an even and fine layer of thickness for the printed structure.

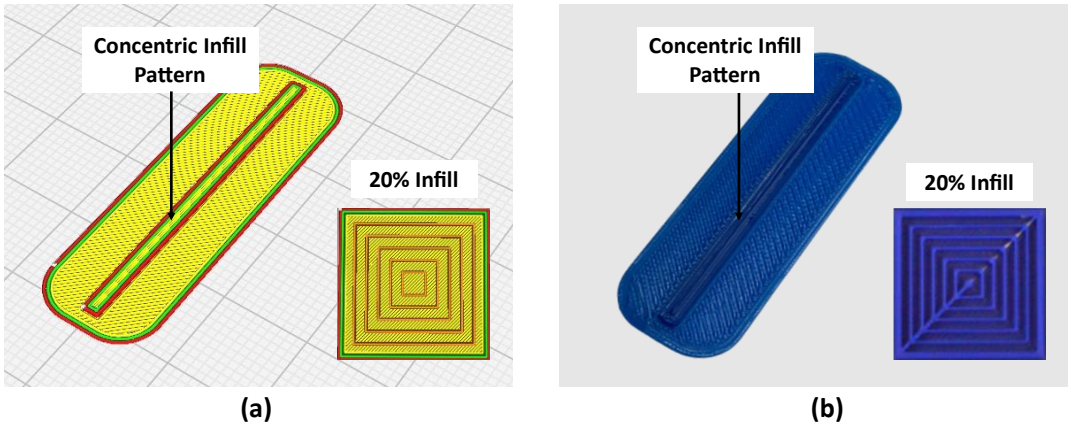

Fig. 3 Illustration of the layer view of the 3D printed structure, showing the 20% concentric infill pattern in (a) Cura slicing software (represented by green and orange parallel lines inside the cuboid structure) and (b) actual picture (represented by dark blue parallel lines inside the cuboid structure).

In terms of nozzle temperature and printing speed, the reason we used different settings for different materials was due to the properties of the material itself, in which each material has its own rate and temperature requirements. The chemical properties of a material influence its melting temperature, which is the temperature at which the material turns from brittle into a rubbery melted substance that the 3D printer's nozzle can extrude. This temperature needs to be achieved for proper printing. Since the materials used in this work have different melting temperatures, each of them needs to be printed at different nozzle temperatures. Printing speed, on the other hand, refers to how quickly the printhead (containing the nozzle of the 3D printer) moves along the X and Y axes while it extrudes the melted material. In general, a faster printing speed will shorten the overall printing time. However, the properties of a material must be considered as it can affect the quality of the printed object. In this work, different printing speeds were used for different materials due to the different modulus of elasticity that each material possesses. This parameter significantly influences their behavior during the printing process, directly impacting the bond between the extruded layers. Materials with higher modulus of elasticity can maintain their shape and bond effectively with adjacent layers, allowing higher printing speeds. This contrasts with softer materials like TPU, necessitating slower speeds to ensure optimal print quality and sensor performance. However, faster speeds can also lead to the accumulation of heat within the printed object, especially for materials that have poor thermal conductivity such as ABS, PC, and TPU. This heat build-up can cause warping, distortion, or other printing issues, which will lead to poor sensor performance. Therefore, to achieve the best print outcome, it is best to adhere to the recommended printing speed specified in each material's specification.

2.2. FBG sensing principle using this design

The sensing element of the FBG-based strain sensor behaves as a wavelength-selective filter that only reflects a specific wavelength when a broadband light source is coupled into the fiber while the rest are being transmitted. The wavelength of the reflected light depends on the periodicity of the grating written on the fiber core, while the bandwidth depends on the grating length, whereby a shorter grating length will allow a broader spectrum to be reflected [35,36]. In this work, the FBGs used are of the uniform, positive-only index change type SMF-28 fiber with a grating length of 1 cm and a reflectivity of ≥ 90%. All FBGs are fabricated in our laboratory using the phase mask technique, where a polymer coating is removed from a fiber segment to expose an ultraviolet interference pattern at its core. This, in return, will create

a periodic change in the refractive index of the FBG gratings, forming the strain sensor. Fundamentally, a light that occupies the same central wavelength as the Bragg wavelength (λ_B) will be reflected by the FBG as shown in Eqn. 1 [4]:

$$\lambda_B = 2n_{eff}\Lambda \tag{1}$$

where λ_B is the reflected Bragg wavelength, n_{eff} is the fiber's effective refractive index, and Λ is the periodicity of the FBG. Any changes in the parameters of strain and temperature will affect the FBG, thus affecting the Bragg wavelength. Therefore, for most industrial applications, the shift given by the Bragg wavelength is affected by both mechanical and thermal strain, as shown by Eqn. 2 [4,26]:

$$\frac{\Delta\lambda_B}{\lambda_B} = \left(1 - p_{eff}\right)\Delta\varepsilon + (\alpha + \xi)\Delta T \tag{2}$$

where p_{eff} is the photoelastic parameter of the fiber material, $\Delta\varepsilon$ the variations in mechanical strain, α represents the coefficient of thermal expansion (CTE) of the fiber material, ξ is the thermo-optic coefficient, and ΔT represents the temperature changes. Since the measurements in this work were conducted in a laboratory environment with a controlled temperature of 26°C, the temperature changes, ΔT are assumed to be $\Delta T \approx 0$. Therefore, there is no need for an additional FBG to provide temperature compensation. So, the Bragg wavelength shift can be directly obtained by:

$$\frac{\Delta\lambda_B}{\lambda_B} = \left(1 - p_{eff}\right)\Delta\varepsilon \tag{3}$$

where the changes in mechanical strain, $\Delta\varepsilon$ can be obtained by simple mathematical calculations giving:

$$\Delta\varepsilon = \frac{\Delta\lambda_B}{\lambda_B\left(1-p_{eff}\right)} \tag{4}$$

3. Laboratory-based calibration of the FBG-based strain sensor

3.1 Setup for comparison of Bragg wavelength shift before and after embedment

The schematic of the setup used to evaluate the Bragg wavelength shift of the FBG-based strain sensors before and after embedment is presented in Fig. 4(a). The FBGs used in

this measurement are presented in Table 3, which shows their respective labeling of the different FBGs, Bragg wavelengths, and the color used to differentiate each of the FBG sensors. The actual picture of the fabricated FBG-based strain sensors is shown in Fig. 4(b). Initially, all 5 different FBG-based strain sensors were individually spliced with a fiber optic pigtail. Then, one of the strain sensors will be connected to Port-2 of the 3-Port circulator as shown in Fig. 4(a), to obtain the initial spectrum of the FBG before embedment. Similar steps were taken with the other 4 strain sensors to get the FBG's spectrum before embedment. Next, all 5 FBG-based strain sensors were embedded inside different materials such as PLA, TPU, PC, ABS, and nylon by positioning the fiber embedding the FBGs through the 3D printed cuboid structure, which was then fixed using cyanoacrylate glue as mentioned in section 2.1. Following that, one of the strain sensors was again connected to Port-2 of the 3-Port circulator to obtain the FBG's spectrum after embedment. The same steps were repeated with the other 4 strain sensors. The responses of all FBGs were taken using a Yokogawa AQ6370C optical spectral analyzer (600 – 1700 nm) with a wavelength resolution set at 0.02 nm and a sampling frequency of 4000Hz, which was connected to Port-3 of the 3-Port circulator. Port-1, on the other hand, was connected to the amplified spontaneous emission (ASE) light source, which will provide a broad spectrum of light for the FBG. The conducted measurements were taken during the day for 2 hours.

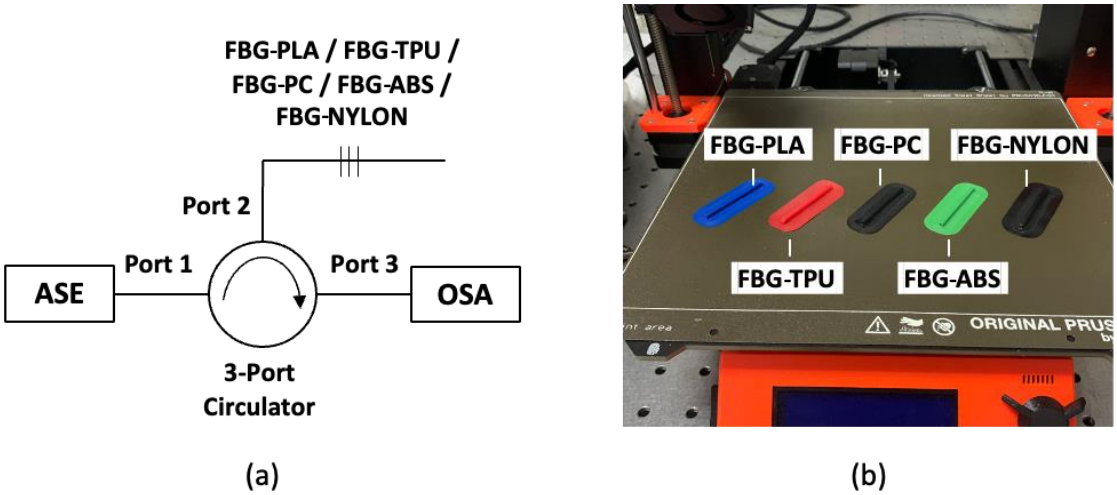

Fig. 4 Illustration of the (a) schematic representation of the interrogation system for the incorporated FBGs (FBG-PLA, FBG-TPU, FBG-PC, FBG-ABS, and FBG-Nylon) and (b) actual picture of the fabricated FBG-based strain sensor

Table 3. FBG names, their respective Bragg wavelengths, and color indicator

FBG Name	Bragg wavelength (nm)	Color Indicator
FBG-PLA	1539.0	Blue
FBG-TPU	1544.0	Red
FBG-ABS	1549.0	Green
FBG-PC	1555.0	Black
FBG-Nylon	1559.0	Black

3.2 Setup for comparison of performance for the embedded FBG-based strain sensors towards varying mechanical strain

In order to perform a comparison of performance between 5 FBGs that have been embedded in 5 different 3D printed materials, a PVC pipe was used to provide a variation of mechanical strain upon bending. The setup to evaluate the FBG's response towards varying mechanical strain can be seen in Fig. 5(a) and (b), showing that the horizontal displacement of the PVC pipe along the optical table can be related to the mechanical strain variation that was obtained by the FBG (positioned 80cm from the fixed end) through the bending of PVC pipe at its free end. First of all, a PVC pipe with a length and diameter of 110 cm and 2 cm respectively, was horizontally laid on the optical table. As the optical table was equipped with a 2D grid of M6-sized holes, one end of the PVC pipe was fixed in position by applying 6 identical M6-typed Allen bolts and a bracket made of stainless steel, as shown in Fig. 5(a), to prevent any form of rotation from taking place on the PVC pipe during measurement. Then, the 5 FBGs of different Bragg wavelengths embedded in various materials (labeled as FBG-PLA, FBG-TPU, FBG-PC, FBG-ABS, and FBG-Nylon) were fixed using a thin double-sided tape (with a thickness of 0.1mm) that covers the whole bottom base of the sensor. This sensor was then placed on the tensile side of the PVC pipe sequentially to allow the measurements of mechanical strain when the pipe was bent at the free end. This means that there will be 5 repeated measurements that comprise 5 different embedded FBG-based sensors. It is also important to take note that the whole underpart of the sensor is in contact with the thin double sided tape. As to certain repeatability of the sensor, each measurement was done in 3 sets.

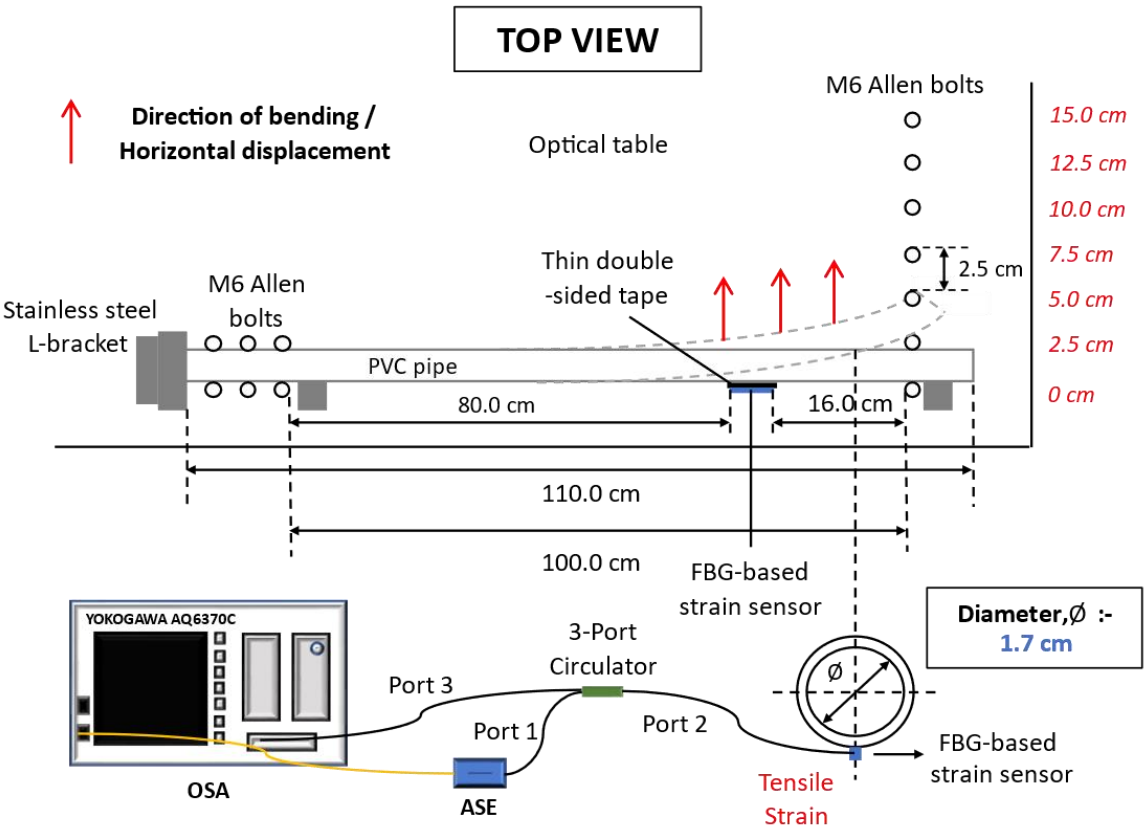
TOP VIEW
Direction of bending / Horizontal displacement
Optical table
M6 Allen bolts
15.0 cm
12.5 cm
10.0 cm
7.5 cm
5.0 cm
2.5 cm
0 cm
2.5 cm
Thin double -sided tape
Stainless steel L-bracket
M6 Allen bolts
PVC pipe
80.0 cm
16.0 cm
110.0 cm
100.0 cm
FBG-based strain sensor
Diameter,Ø :- 1.7 cm
YOKOGAWA AQ6370C
3-Port Circulator
Port 3
Port 1
Port 2
Ø
FBG-based strain sensor
OSA
ASE
Tensile Strain

(a)

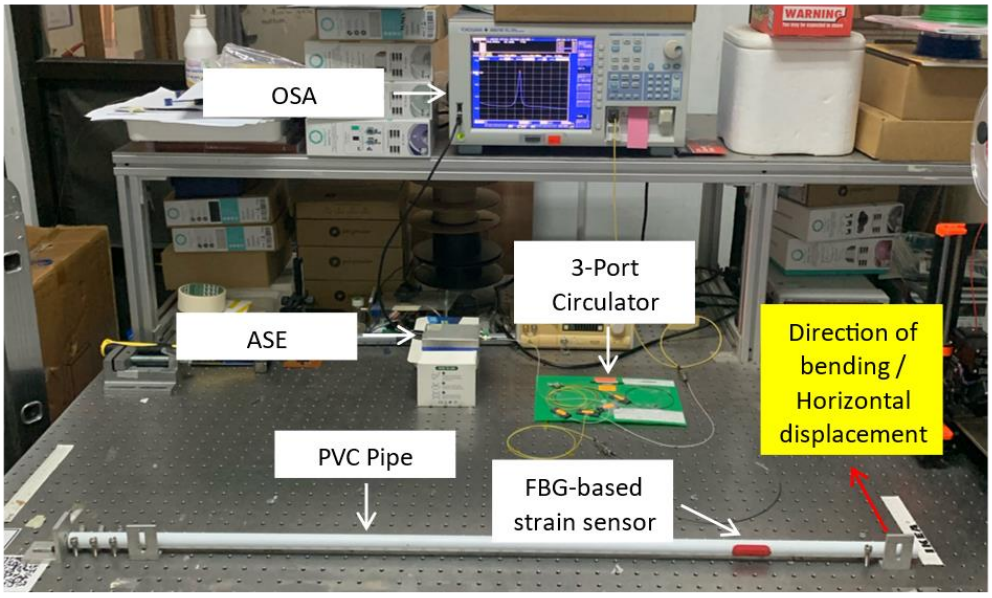
OSA
3-Port Circulator
ASE
Direction of bending / Horizontal displacement
PVC Pipe
FBG-based strain sensor

(b)

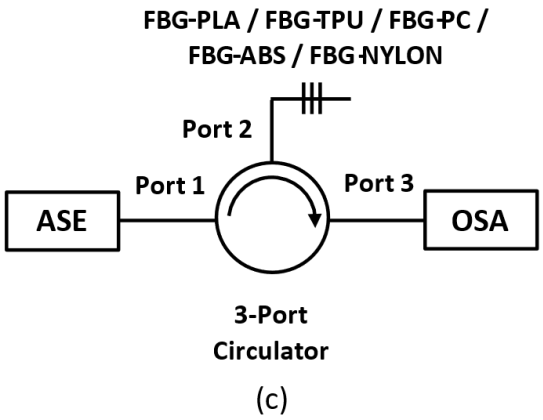

(c)

Fig. 5 Illustration of the (a) laboratory setup and (b) actual setup for the comparison of performance for the embedded FBG-based strain sensors towards varying mechanical strain, and (c) schematic diagram of the interrogation system for the incorporated FBGs (FBG-PLA, FBG-TPU, FBG-PC, FBG-ABS, and FBG-Nylon)

Fig. 5(c) shows the schematic diagram of the interrogation system used in this measurement. Similarly to the measurements conducted in *Section 3.1*, the same Yokogawa AQ6370C optical spectral analyzer (600 – 1700 nm) was used to observe the response of all FBGs where it was connected to Port-3 of the 3-Port circulator. Each FBG was connected to Port-2 in turn, while an amplified spontaneous emission (ASE) light source was connected to Port-1 of the 3-Port circulator. The performance of each FBG's response was evaluated based on the horizontal displacement of the free end of the pipe over the range of 0 to 15 cm, where the bending direction is shown in Fig. 5(a). As this was done in turn, the measurements were taken for one FBG at a time to compare the performance of each FBG, which was embedded in different 3D printed materials. Upon comparison, a validation on which materials were suitable to be used as a reliable strain sensor can be established.

3.3 Temperature sensitivity determination on each of the embedded FBG-based strain sensor

As each FBG used in this work was embedded in different materials, it was also crucial to determine the response of each material towards the temperature change. Each of the FBG-based strain sensors was immersed inside a water bath, as illustrated in Fig. 6. From the figure, the end of the FBG fiber was placed through the hole of a washer nut and taped at the bottom of the water bath using a waterproof flex tape. It prevents the sensor from floating in the water

bath during measurement. Next, for the measurements to be undertaken, the temperature of the water bath was initially set at room temperature (26°C), which was then progressively increased in 10°C intervals over the range of 26°C to 80°C. Concurrently, the Bragg wavelength shift of each FBG (connected to Port-2 of the 3 Port-circulator) was measured and recorded using an OSA. It is vital to take note that the measurements were taken on each FBG one after another, which also means that there will be 5 repeated measurements that comprise 5 different embedded FBG-based sensors. Each measurement is done in 3 sets in order to test the repeatability of the sensor towards varying temperatures.

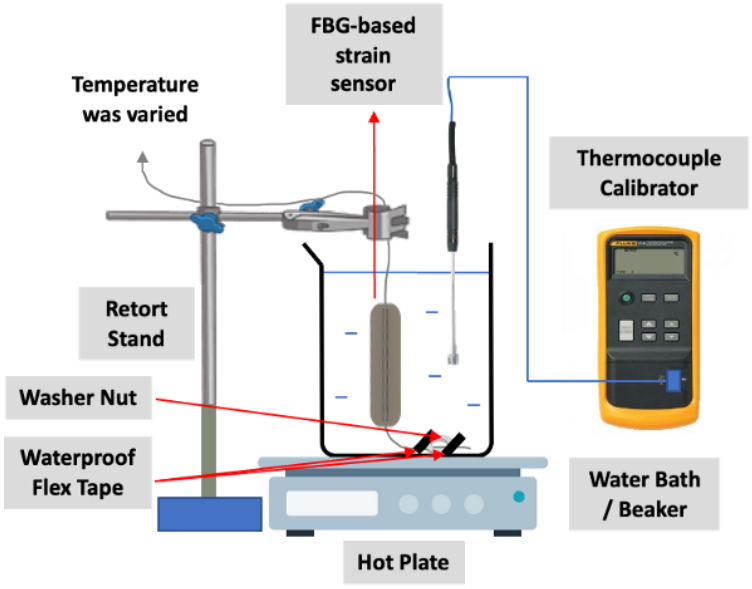

Fig. 6 Setup for temperature sensitivity determination for the incorporated FBG-based strain sensors (FBG-PLA, FBG-TPU, FBG-PC, FBG-ABS, and FBG-Nylon)

4. Evaluation of FBG-based strain sensors response in small-scale field test

4.1 Sensor protection scheme

To ensure optimal performance of the embedded FBG-based strain sensors during small-scale field testing, it was essential to provide them with reliable protection, as illustrated in Fig. 7(c). This was achieved using a high-quality self-fusing silicone rubber tape from WALTEK (Fig. 7(a)), which was selected for its exceptional properties. It includes impressive waterproofing and moisture resistance, high flexibility, and a wide operating temperature range (-60°C to +200°C). This tape provides a watertight seal with remarkable instantaneous fusion capabilities, making it ideal for sealing materials in various applications. The application of the tape to the embedded FBG-based strain sensors can be observed in Figs. 7(b) and (c),

respectively. Previous research by Alias *et al.* [28] also demonstrated the tape's effectiveness in safeguarding the FBG-based strain sensors embedded in a 3D-printed TPU structure, resulting in ~1.13 times enhancement in sensor sensitivity. Furthermore, to enhance waterproofing, a nylon protective cloth (Fig. 7(d)) was wrapped around the PVC pipe's entire length (Fig. 7(e)). In contrast, an additional layer of black plastic sheeting (Fig. 7(d)) was applied to the outer section of the PVC pipe (Fig. 7(f)), providing a smoother surface upon installation and preventing soil moisture interference that may affect the sensor's reading.

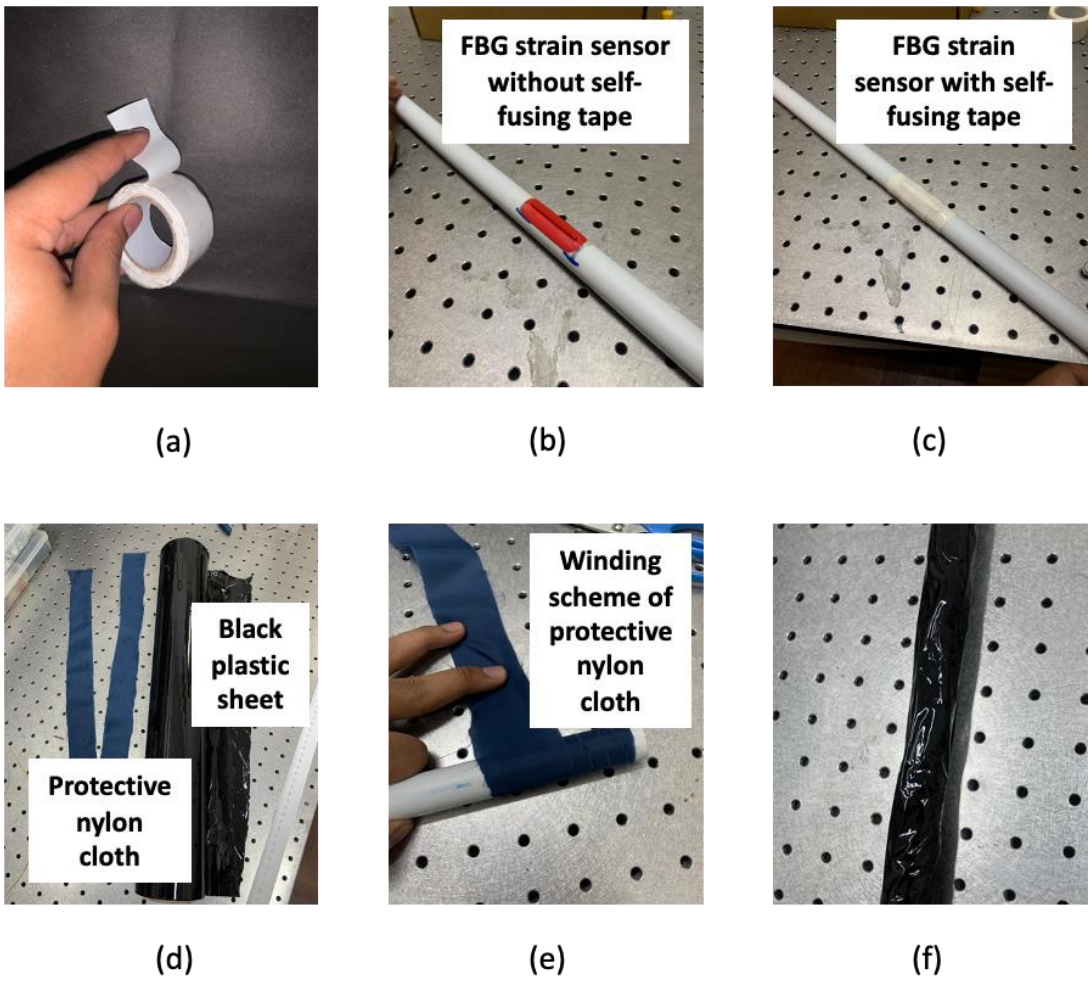

Fig. 7 Illustration of the actual picture of (a) WALTEK silicone self-fusing tape, (b) FBG strain sensor without self-fusing tape, (c) FBG strain sensor with self-fusing tape, (d) protective nylon cloth and black plastic sheet, (e) the winding scheme of protective nylon cloth, and (f) PVC pipe after wrapping with a black plastic sheet.

4.2 Temperature compensation mechanism

To provide temperature compensation during the small-scale field test, an additional FBG (referred to as FBG T) was added in the setup. It is important to take note that the material and dimension used to embed FBG T should be the same as the FBG-based strain sensor during the measurement, as different materials would respond differently towards temperature due to the CTE that each material possess. This is to ensure that a reliable temperature-compensating sensor can be applied effectively. Next, when measurement was conducted on FBG-PLA, FBG T will be a similar type to that of the strain sensor. The only difference is that FBG-PLA is strain-sensitive while FBG T is strain-free, as it should not be affected by any strain variations. Therefore, there should be an additional 5 FBG T which were labelled as FBG T-PLA, FBG T-TPU, FBG T-PC, FBG T-ABS, and FBG T-Nylon. The Bragg wavelength of each FBG T is given in Table 4. Each FBG T was protected by housing in a specially designed casing termed as 'FBG T joint' (as shown in Fig. 8(a)). The FBG T joint, made from PLA material using 3D printing, was positioned at rigid points that remained free from strain at each end of the PVC pipe. FBG T was then inserted through the holes in the FBG T joint and remained loose inside the pipe to solely measure temperature changes without being affected by strain. The FBG T was safeguarded by having an additional cover (labeled as FBG T joint cap), which was fabricated using PLA material to seal the joint effectively. The dimensions of the FBG T joint cap utilized in this work are presented in Fig. 8(b).

Table 4. Bragg wavelength for all FBG T

FBG T	Bragg wavelength (nm)
PLA	1537.0
TPU	1541.0
PC	1547.0
ABS	1551.0
Nylon	1557.0

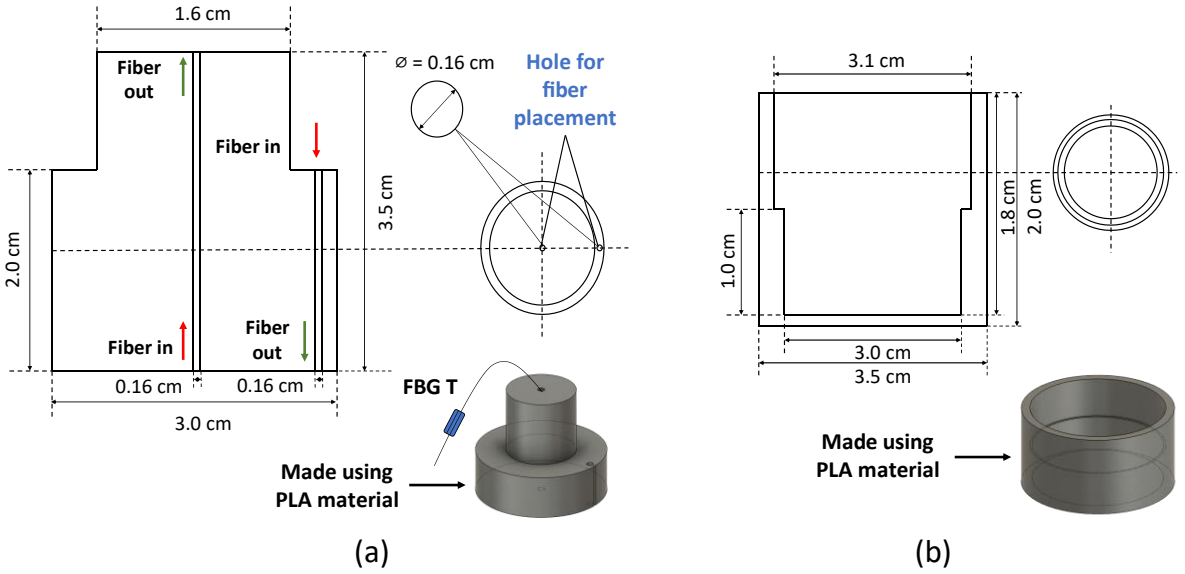

Fig. 8 Illustration of the (a) FBG T joint with FBG T and (b) FBG T joint cap (protective cover) showing their key dimensions

4.3 Temperature characterization for FBG T

The temperature characterization on the FBG T (FBG T-PLA, FBG T-TPU, FBG T-PC, FBG T-ABS, and FBG T-Nylon) was performed using a water bath calibration method similar to the procedure in *Section 3.3*. The FBG sensors were placed inside the water bath, initially set at room temperature (26°C), and the temperature was then gradually increased in 10°C intervals up to 80°C. The wavelength shifts of the FBG sensors were observed and recorded using an OSA. It is important to note that the measurements were conducted sequentially on each FBG T, resulting in five repeated measurements corresponding to FBG T-PLA, FBG T-TPU, FBG T-PC, FBG T-ABS, and FBG T-Nylon, respectively.

4.4 Setup for small-scale field test

The setup used to evaluate the response of the FBG-based strain sensor during field testing is depicted in Fig. 9(a). This setup allows the bending of the 168 cm PVC pipe at the bending point (82 cm from each fixed end), simulating soil movements by applying known forces through weights, thus inducing strain variations that can be monitored. For testing, the PVC pipe was suspended in the middle of a 175 cm x 50 cm x 50 cm container using 3D printed PVC pipe holders screwed into the wood, providing rigid points at both ends. Cloth tape was tightly wrapped around each end of the PVC pipe to prevent rotation during testing. The location of the FBG-based strain sensor was marked on the cloth tape, as shown in Fig. 9(b),

before burying the PVC pipe 10 cm below ground. The ground level was monitored using a measuring tape attached to the inner walls of the wooden box.

The optical interrogation setup consisted of an amplified spontaneous emission light source connected to Port-1 of the 3-port circulator. The serially-spliced FBGs (FBG strain sensor and FBG T) were attached to the body of the PVC pipe, which was connected to Port 2. Port 3 was linked to a Yokogawa AQ6370C optical spectrum analyzer (OSA) to measure the response of the FBG to applied forces using weights ranging from 1 kg to 10 kg, placed directly on the soil above the FBG's location. The soil moved downward due to the gravitational force, as illustrated in Fig. 9(a).

In the experiment, the response of each FBG-based strain sensor was measured by incrementally increasing weights from 1 kg to 10 kg on the FBG PLA. The same steps were repeated for FBG-TPU, FBG-PC, FBG-ABS, and FBG-Nylon. FBG T, on the other hand (such that FBG T-PLA, FBG T-TPU, FBG T-PC, FBG T-ABS, and FBG T-Nylon), will not be affected by the applied weights as it was positioned loosely inside the PVC pipe, thus providing the ability to correct any temperature effects. These tests were conducted from 4.00 p.m. to 6.30 p.m., where the surrounding temperature was recorded at 27.5°C.

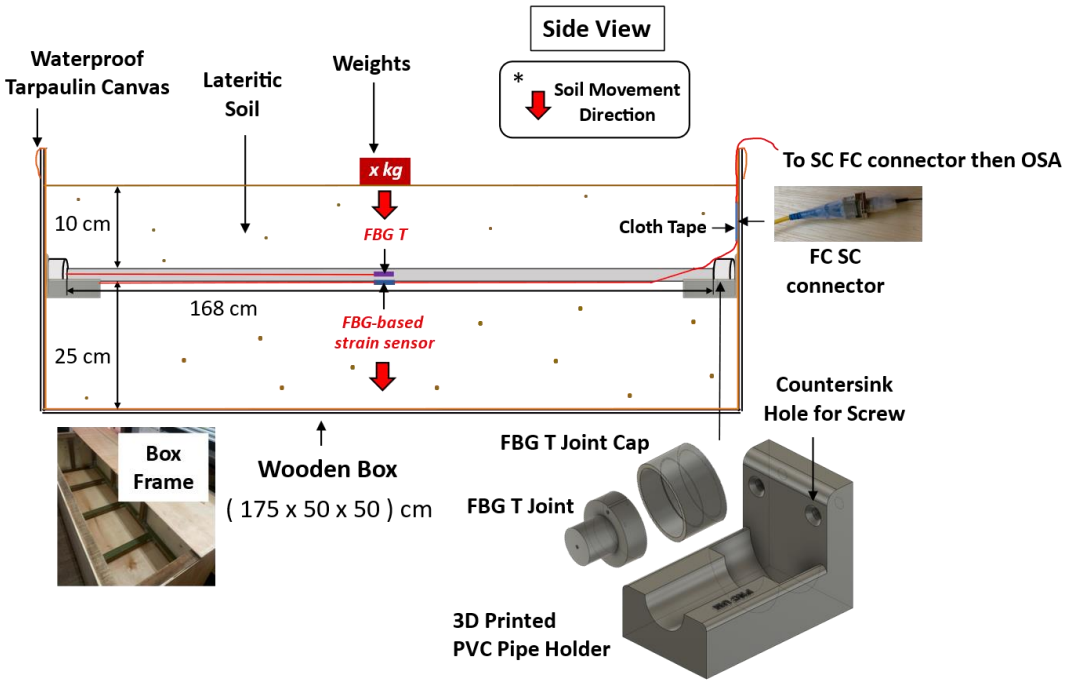

(a)

(b)

Fig. 9 Illustration of the (a) small-scale field test setup, and (b) visual depiction of field testing in progress

5. Results and Discussion

5.1 Comparison of Bragg wavelength shift before and after embedment

Fig. 10 illustrates the reflected spectrum of all utilized FBGs before and after embedment. The difference in wavelength shifts before and after embedment are also presented in Table 5. Based on Fig. 10(a), (c), (d), (e), and Table 5, it was observed that the Bragg wavelengths for all FBGs experience a blueshift of 0.190 nm, 0.035 nm, 0.023 nm, and 0.103 nm respectively. However, in the case of Fig. 10(b) with reference to Table 5, the Bragg wavelength for the TPU-embedded FBG-based strain sensor moves to longer wavelengths at about 0.134 nm (redshift) where the measurement had been repeated several times. It is different from the other embedded FBG-based strain sensors as it experiences redshift instead of blueshift. The reason for such redshift could have been due to the pre-stressing process of the FBG inside the 3D printed TPU structure as well as the properties of the TPU material itself. Since TPU is known to be a flexible material, the gratings of the FBG might have been stretched when a cyanoacrylate adhesive was applied. The same phenomenon can be observed in the work by Ahmad *et al.* [4], where the FBG also experiences a redshift (0.136 nm) upon embedment inside a TPU structure, which also has an infill density of 20%, similar to this work.

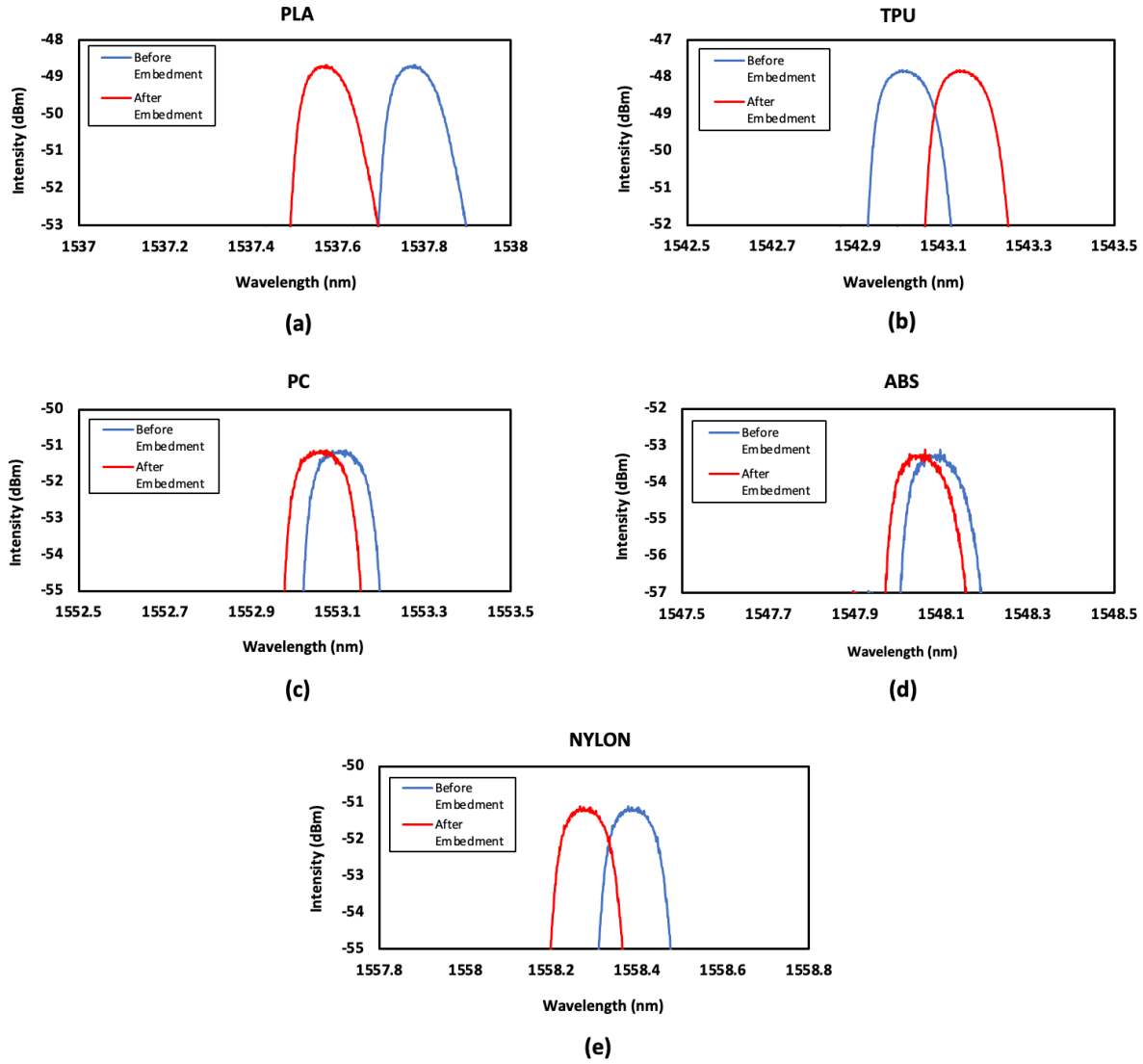

Fig. 10 Illustration of the wavelength shift before and after embedment for (a) FBG-PLA, (b) FBG-TPU, (c) FBG-PC, (d) FBG-ABS, and (e) FBG-Nylon

Table 5. Difference in the Bragg wavelength shift before and after embedment for all FBGs

FBG	Difference in Bragg wavelength shift before and after embedment (nm)
FBG-PLA	0.190
FBG-TPU	0.134
FBG-PC	0.035
FBG-ABS	0.023
FBG-Nylon	0.103

5.2 *Comparison of performance for the embedded FBG-based strain sensors towards varying mechanical strain*

Fig. 11 shows the spectrum of all 5 FBGs (FBG-PLA, FBG-TPU, FBG-PC, FBG-ABS, and FBG-Nylon) in response to varying horizontal displacement. Based on the measurements, the graph in Fig. 12 shows a satisfactory linear response with a small standard deviation and a high average R^2 value equal to 0.9845 for all FBGs, with FBG TPU obtaining the highest mechanical strain sensitivity with a value of 17.7 pm/cm of displacement. The higher Young's modulus value of a material, the greater the rigidity of the material. For those materials with a higher Young's modulus, they would require more force to be applied to produce a given deformation. A material that has a higher Young's modulus value is considered to be less elastic (brittle) than a material that has a lower Young's modulus value (ductile). Brittle materials tend to be strong because they can withstand a lot of stress, would not stretch very much, and would break suddenly, while ductile materials are more elastic because they have a larger elastic region.

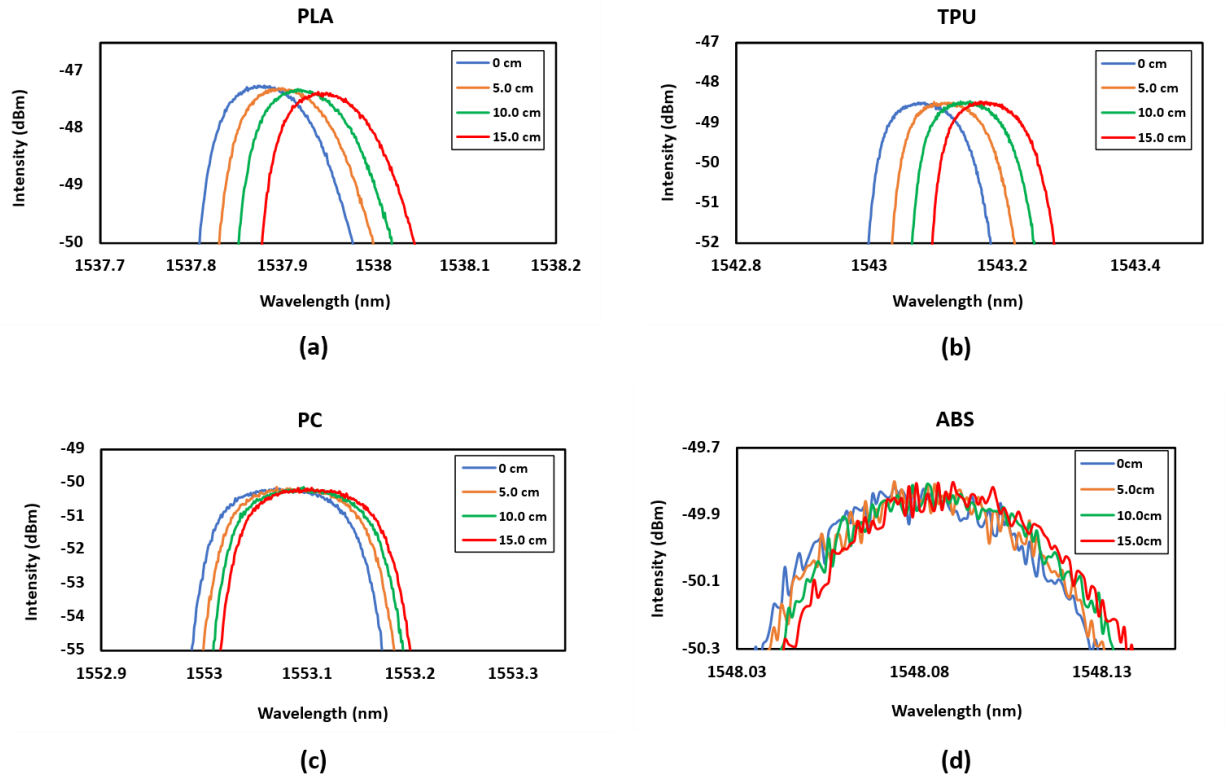

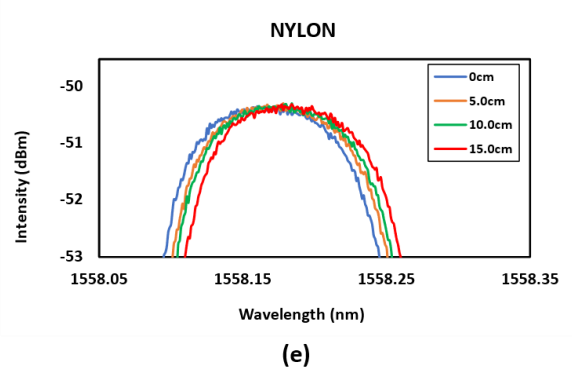

Fig. 11 Illustration of the wavelength spectrum for FBG-based strain sensor embedded in (a) PLA, (b) TPU, (c) PC, (d) ABS, and (e) Nylon filament

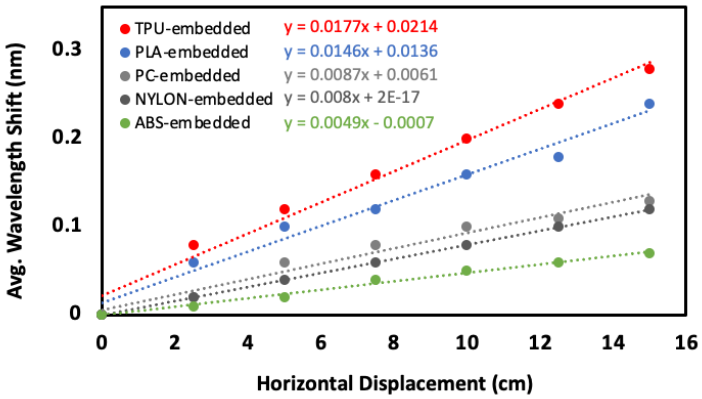

Fig. 12 Illustration of the average mechanical strain sensitivity for each of the incorporated FBG-based strain sensors (FBG PLA, FBG TPU, FBG PC, FBG ABS, and FBG Nylon)

This shows that TPU is more ductile and more elastic compared to other materials (PLA, PC, ABS, and nylon). Hence, the FBG that was embedded in a TPU-based structure would show greater wavelength shifts (enhanced sensitivity), as seen in Fig. 12, compared to the other FBGs that were embedded in PLA, PC, ABS, and nylon. It is also because the TPU-based structure could stretch more and induce larger strain to the FBG (larger wavelength shifts) compared to the other materials when the same amount of force was applied. From Table 6, we can see that FBGs that were embedded inside materials with high Young's Modulus tend to have a lower mechanical strain sensitivity due to the rigidity of the material itself. This is the reason for the results obtained in Fig. 12, which indicates that the mechanical strain sensitivity of FBG-TPU > FBG-PLA > FBG-PC > FBG-Nylon > FBG-ABS, thus showing that TPU is the best choice for applications that require high mechanical strain sensitivity.

Table 6. Mechanical strain sensitivity for all embedded FBGs

FBG Name	Young's Modulus (GPa)	Mechanical Strain Sensitivity (pm/cm)				Standard Deviation (σ)	R-Squared Value
		1st Reading	2nd Reading	3rd Reading	Avg. Reading		
FBG-PLA	1.80	14.6	14.5	14.7	14.6	0.1000	0.9793
FBG-TPU	0.02	17.7	17.6	17.7	17.7	0.0577	0.9846
FBG-PC	2.00	8.8	8.7	8.6	8.7	0.1000	0.9710
FBG-ABS	2.90	4.9	4.7	5.0	4.9	0.1528	0.9897
FBG-Nylon	2.20	8.0	7.8	8.1	8.0	0.1528	0.9980

5.3 Temperature sensitivity of each of the embedded FBG-based strain sensor

From Fig. 13, the average temperature sensitivities for FBG-PLA, FBG-TPU, FBG-PC, FBG-ABS, and FBG-Nylon are 12.5 pm/°C, 15.4 pm/°C, 13.2 pm/°C, 13.8 pm/°C, and 14.1 pm/°C respectively, having a small standard deviation and an excellent linearity value of up to 99%. Based on the measurement, it indicates that TPU possesses the highest temperature sensitivity compared to its other counterparts, such as the temperature sensitivity of FBG-TPU > FBG-Nylon > FBG-ABS > FBG-PC > FBG-PLA. This is due to the higher coefficient of thermal expansion (CTE) that TPU exhibits, with a value of 100 x 10^{-6}/°C [30]. Materials that have a high CTE value will have the capability to expand more as temperature increases, which, in return, induces more strain on the FBG gratings. The same principles were also applied to the other embedded FBG-based strain sensors (for FBG-PLA, FBG-PC, FBG-ABS, and FBG-Nylon), as each of the materials carries a different CTE. Table 7 presents the temperature sensitivity of each FBG as well as the CTE of the materials that were used to embed the FBG. The temperature sensitivity of bare FBG was also included in Fig. 13 and Table 7 to serve as a reference for the embedded FBGs, giving a standard value of 11.0 pm/°C (lowest sensitivity compared to the embedded FBGs) [28]. Therefore, any industrial applications that require a strain sensor with high-temperature sensitivity can be made possible by embedding an FBG in a TPU structure, as it carries a temperature sensitivity that is ~1.74 times higher than a bare FBG. Meanwhile, materials such as PLA, PC, ABS, and nylon can also be considered according to the suitability of the application.

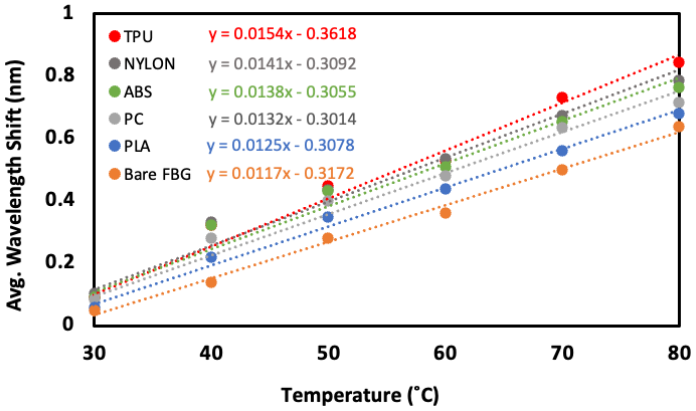

Fig. 13 Illustration of the average temperature sensitivity for each of the incorporated FBG-based strain sensors (FBG-PLA, FBG-TPU, FBG-PC, FBG-ABS, and FBG-Nylon) as well as a bare FBG sensor

Table 7. Temperature sensitivity for all embedded FBGs and bare FBG

FBG Name	Coefficient of Thermal Expansion (10^{-6}/°C)	Temperature Sensitivity (pm/°C)				Standard Deviation (σ)	R-Squared Value
		1st Reading	2nd Reading	3rd Reading	Avg. Reading		
FBG-PLA	68.0	12.5	12.5	12.4	12.5	0.0577	0.9922
FBG-TPU	100.0	15.3	15.6	15.4	15.4	0.1528	0.9812
FBG-PC	69.0	13.2	13.1	13.2	13.2	0.0577	0.9780
FBG-ABS	90.0	13.8	13.7	13.9	13.8	0.1000	0.9699
FBG-Nylon	95.0	14.1	14.3	14.0	14.1	0.1528	0.9718
Bare FBG	0.5	11.0	11.0	11.1	11.0	0.0577	0.9953

5.4 *Small-scale field test*

The evaluation of the FBGs response in below-ground conditions was conducted using the setup depicted in Fig. 9. Initially, the wavelength shifts of all FBGs were monitored before and after being buried below ground. For example, the response of FBG-PLA and FBG T-PLA, which represent a strain-sensitive FBG and a strain-insensitive FBG respectively, can be seen in Fig. 14(a) where FBG-PLA exhibited a blueshift of 0.20 nm after being buried below ground,

indicating a shift to the left. The blueshift experienced by FBG-PLA suggests a decrease in surrounding temperature, which affects the gratings of the strain-sensitive FBG caused by both temperature and strain variations.

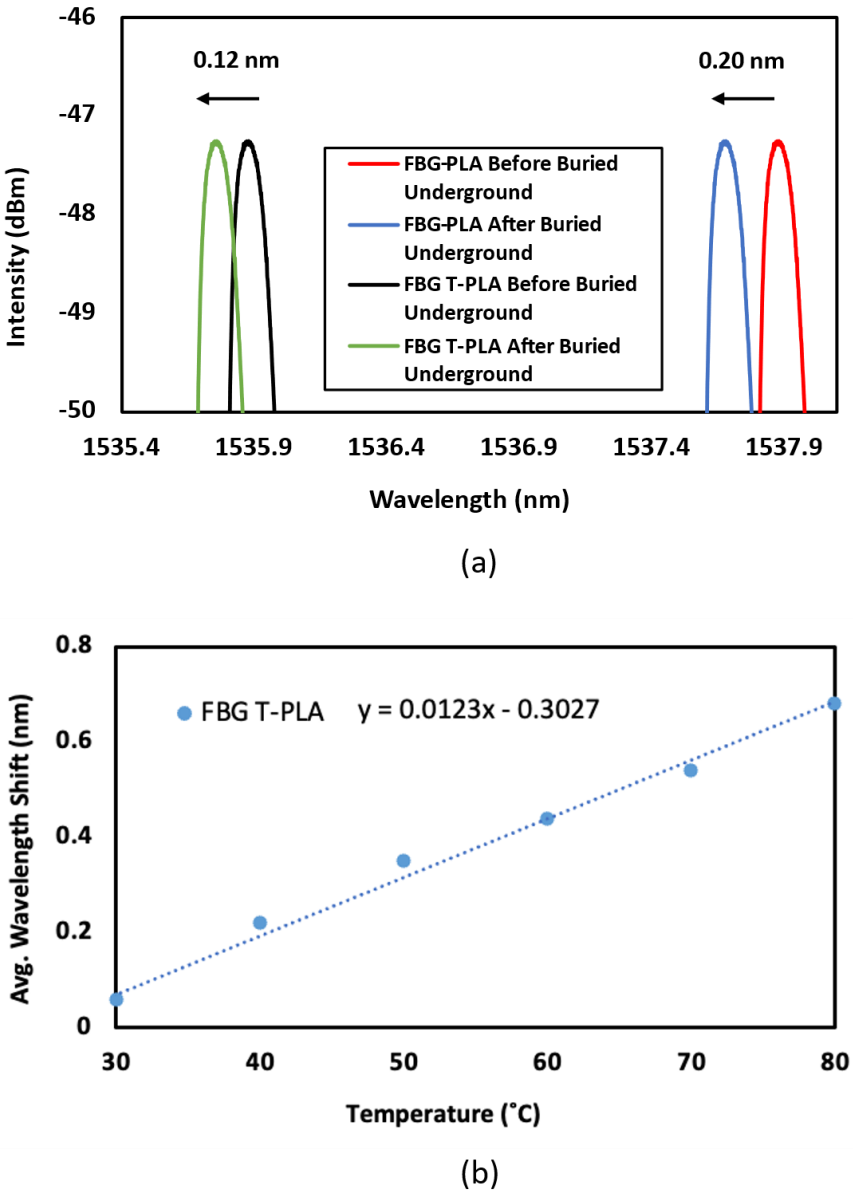

Fig. 14 Illustration of the (a) wavelength shift of FBG-PLA and FBG T-PLA before and after being buried below ground and (b) average temperature sensitivity of FBG T-PLA

For compensation of the temperature effect, the wavelength shift of FBG-PLA was subtracted from the wavelength shift obtained by FBG T-PLA, which was observed to be shifted to the left by 0.12 nm after burying below ground. Since FBG T-PLA only experiences temperature changes due to the decrease in surrounding temperature, it can perform as a

suitable temperature sensor for compensation purposes. Therefore, by subtracting 0.12 nm from the data obtained in FBG T-PLA, accurate strain measurements can be derived from FBG-PLA. The temperature sensitivity of FBG T-PLA, as depicted in Fig. 14(b), was determined as 12.3 pm/°C. The same analysis was done on FBG-TPU and FBG T-TPU, FBG-PC and FBG T-PC, FBG-ABS, and FBG T-ABS, as well as FBG-Nylon and FBG T-Nylon, where the results are presented in Fig. 15 (a) and (b) respectively.

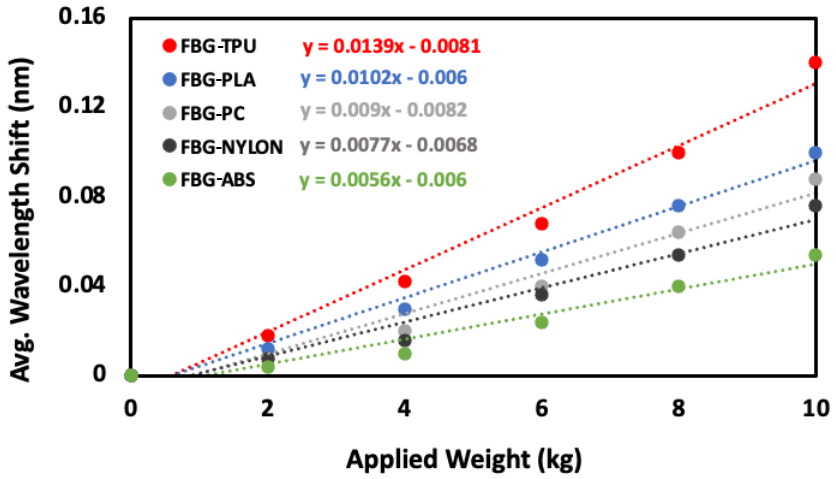

(a)

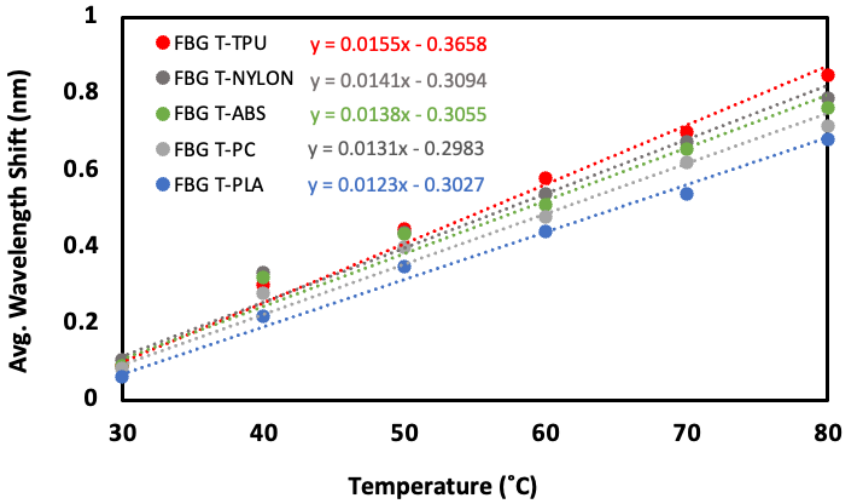

(b)

Fig. 15 Illustration of the (a) average wavelength shift (nm) against applied weight (kg) and (b) average wavelength shift (nm) against temperature (°C) for all FBGs

Fig. 15(a) provides a visual representation indicating that the FBGs displaying the largest average wavelength shifts are those subjected to the highest levels of induced strain as

a result of the applied weights. FBG-TPU exhibits the largest wavelength shift, followed by FBG-PLA, FBG-PC, FBG-Nylon, and FBG-ABS. The reason behind this is due to the low Young's Modulus value of the TPU material, which is 29 MPa [31]. Table 8 provides the mechanical strain sensitivity of all strain-sensitive FBGs (FBG-PLA, FBG-TPU, FBG-PC, FBG-ABS, and FBG-Nylon), where Δwl refers to the difference in Bragg wavelength before and after burying below ground. The table reveals a small standard deviation in the measurements, indicating consistent and reliable results. Additionally, the FBGs demonstrate good linearity values, further validating their accuracy.

Table 8. Mechanical strain sensitivity for all strain-sensitive FBGs

FBG Name	Δwl (nm)	Mechanical Strain Sensitivity (pm/kg)				Standard Deviation (σ)	R-Squared Value
		1st Reading	2nd Reading	3rd Reading	Avg. Reading		
FBG-PLA	0.20	10.2	10.2	10.3	10.2	0.0577	0.9876
FBG-TPU	0.24	14.0	13.8	13.9	13.9	0.1000	0.9822
FBG-PC	0.19	8.8	9.0	9.0	8.9	0.1155	0.9652
FBG-ABS	0.16	5.2	6.0	5.6	5.6	0.4000	0.9636
FBG-Nylon	0.20	7.8	8.0	7.4	7.7	0.3055	0.9528

Fig. 15(b) shows the average temperature sensitivity for all FBG T (FBG T-PLA, FBG T-TPU, FBG T-PC, FBG T-ABS, and FBG T-Nylon). According to the information presented in the figure, it can be observed that FBG T-TPU possesses the highest temperature sensitivity compared to its other counterparts such that the temperature sensitivity of FBG T-TPU > FBG T-Nylon > FBG T-ABS > FBG T-PC > FBG T-PLA. Table 9 shows the temperature sensitivity for all FBG T, such that FBG T-PLA, FBG T-TPU, FBG T-PC, FBG T-ABS, and FBG T-Nylon respectively. From the table, it becomes evident that the measurement conducted resulted in a small standard deviation, indicating a repeatable measurement. Additionally, the linearity values exhibit a strong response, reaching up to 99%, which demonstrates the reliability and accuracy of the measurements.

Table 9. Temperature sensitivity for all FBG T

FBG Name	Δwl (nm)	Temperature Sensitivity (pm/°C)				Standard Deviation (σ)	R-Squared Value
		1st Reading	2nd Reading	3rd Reading	Avg. Reading		
FBG T-PLA	0.12	12.3	12.3	12.4	12.3	0.0577	0.9904
FBG T-TPU	0.16	15.5	15.6	15.5	15.5	0.0577	0.9867
FBG T-PC	0.12	13.3	13.1	13	13.1	0.1528	0.9782
FBG T-ABS	0.08	13.8	13.8	13.9	13.8	0.0577	0.9699
FBG T-Nylon	0.12	14.1	14.2	14.0	14.1	0.1000	0.9719

5. Conclusions

In this work, an optical fiber Bragg grating (FBG)-based strain sensor was developed using 3D printing technology. It has been demonstrated that FBG will respond differently upon embedment in different 3D printed materials in terms of both mechanical strain and temperature changes. Based on the obtained data, it can be seen that TPU-embedded FBG gives the best mechanical strain sensitivity compared to its other counterparts, giving a value of 17.70 pm/cm of displacement with a high linearity value of 98%. The least preferable response was from the ABS-embedded FBG, which only gives a mechanical strain sensitivity of 4.90 pm/cm of displacement (~3.6 times lower than TPU-embedded FBG) due to the high Young's Modulus value that ABS material has. In terms of temperature sensitivity, TPU-embedded FBG has the highest temperature sensitivity with a value of 15.4 pm/°C, which was ~1.74 times higher than that of the bare FBG. It was also due to its high CTE (100.0 x 10^{-6}/°C), which allows the TPU structure to expand more upon heating, thus stretching the FBG gratings inside. On the other hand, PLA-embedded FBG gives the least temperature sensitivity with a value of 12.5 pm/°C, which is ~1.23 times lower than that of the TPU-embedded FBG. In addition, during small-scale field testing conducted in below-ground environments, the application of TPU-embedded FBGs as strain sensors has proven to be highly effective. These sensors exhibited a responsivity of 13.9 pm/kg, along with a standard deviation of not more than 0.40, indicating consistent, repeatable, and reliable performance. Additionally, the strain sensors demonstrated high

linearity, further confirming their accuracy and predictable behavior. This substantiates TPU as the optimal material choice for applications necessitating heightened sensitivity to both mechanical and temperature variations, such as ground movement monitoring. The other materials can also be considered according to the sensitivity requirements and suitability of the application. The proposed method using 3D-printed structures to embed the FBGs is an inexpensive process, and the cost of the 3D-printed sensors could be lower than sensors by other means due to the cheaper raw materials used.

6. Acknowledgements

A Newton Fund Impact Scheme grant, ID IF022-2020, under the Newton-Ungku Omar Fund partnership supported this work. The grant is funded by the UK Department for Business, Energy and Industrial Strategy and the Malaysian Industry-Government Group for High Technology (MIGHT). Grattan also acknowledges the support from the Royal Academy of Engineering. Universiti Malaya also supported this work under the grant BKS002-2023 and IIRG001A-2023.

7. References

[1] K. T. V Grattan and T. Sun, "Fiber optic sensor technology: an overview," *Sensors and Actuators A: Physical*, vol. 82, no. 3, pp. 40–61, May 2000, doi: 10.1016/S0924-4247(99)00368-4.

[2] H. K. Hisham, "Optical fiber sensing technology: Basics, classifications and applications, " *American Journal of Remote Sensing*, vol. 6, no. 1, pp. 1–5, June 2018, doi: 10.11648/j.ajrs.20180601.11.

[3] Q. Zhang, Y. Wang, and Y. Sun, "Using custom fiber Bragg grating-based sensors to monitor artificial landslides," *Journal of Sensors*, vol. 16, no. 9, pp. 1–13, Aug. 2016, doi: 10.3390/s16091417.

[4] H. Ahmad, M. A. Alias, M. F. Ismail, N. N. Ismail, M. K. A. Zaini, K. S. Lim, G. Brambilla, K. T. V. Grattan, and B. M. A. Rahman, "Strain sensor based on embedded fiber Bragg grating in thermoplastic polyurethane using the 3D printing technology for improved sensitivity," *Photonic Sensors*, vol. 12, no. 3, pp. 1–11, Sep. 2022, doi: 10.1007/s13320-021-0646-1.

[5] W. Zhang, G. Kai, X. Dong, S. Yuan, and Q. Zhao, “Temperature-independent FBG-type torsion sensor based on combinatorial torsion beam,” *IEEE Photonics Technology Letters*, vol. 14, no. 8, pp. 1154–1156, Aug. 2002, doi: 10.1109/LPT.2002.1022000.

[6] W. Zhang, Q. Tu, E. Li, J. Xi, J. Chicharo, G. Y. Kai, S. Yuan, X. Dong, “Temperature-independent FBG-type torsion sensor, ” *Proc. of SPIE, Asia-Pacific Optical Communications Conference 2005, Passive Components and Fiber-based Devices II*, vol. 6019, pp. 1–4, Dec. 2005, doi: 10.1117/12.634919.

[7] M. A. Alias, M. F. Ismail, M. S. M. Sa'ad, M. K. A. Zaini, K. S. Lim, K. T. V. Grattan, G. Brambilla, B. M. A. Rahman, S. A. Reduan, and H. Ahmad, "A high-precision extensometer system for ground displacement measurement using fiber Bragg Grating," *IEEE Sensors Journal*, vol. 22, no. 9, pp. 8509-8521, Mar. 2022, doi: 10.1109/JSEN.2022.3159850.

[8] Y. L. Wang, B. Shi, T. L. Zhang, H. H. Zhu, Q. Jie, and Q. Sun, “Introduction to an FBG-based inclinometer and its application to landslide monitoring,” *Journal of Civil Structural Health Monitoring*, vol. 5, no. 5, pp. 645–653, July 2015, doi: 10.1007/s13349-015-0129-4.

[9] A. B. Huang, C. C. Wang, J. T. Lee, and Y. T. Ho, “Applications of FBG-based sensors to ground stability monitoring,” *Journal of Rock Mechanics and Geotechnical Engineering*, vol. 8, no. 4, pp. 513–520, Aug. 2016, doi: 10.1016/j.jrmge.2016.01.007.

[10] L. Yan, Z. Wu, Z. Zhang, W. Pan, B. Luo, and P. Wang, “High-speed FBG-based fiber sensor networks for semi distributed strain measurements,” *IEEE Photonics Journal*, vol. 5, no. 2, pp. 1–7, Apr. 2013, doi: 10.1109/JPHOT.2013.2258143.

[11] H. H. Zhu, B. Shi, and C. C. Zhang, “FBG-based monitoring of geohazards: Current status and trends,” *Sensors*, vol. 17, no. 3, pp. 132–144, Feb. 2017, doi: 10.3390/s17030452.

[12] Z. Lu, C. Hong, Y. Zhang, D. Su, and Y. Fu, “Development of an FBG sensor for measuring large range and multi-directional settlement,” *IEEE Photonics Journal*, vol. 7, no. 8, pp. 107669–107677, Aug. 2019, doi: 10.1109/ACCESS.2019.2932774.

[13] Y. Zhao and F. Ansari, “Quasi-distributed fiber-optic strain sensor: principle and experiment,” *Applied Optics*, vol. 40, no. 19, pp. 3176–3181, July 2001, doi: 10.1364/AO.40.003176.

[14] P. Ferdinand, S. Magne, V. Dewyter-Marty, C. Martinez, S. Rougeault, and M. Bugaud, “Applications of Bragg grating sensors in Europe, ” *12th International Conference on*

Optical Fiber Sensor, Optical Society of America Technical Digest Series, vol. 16, no. 1, pp. 14–19, Oct. 1997, doi: 10.1364/OFS.1997.OTuB1

[15] L. Xu, N. Liu, J. Ge, X. Wang, and M. P. Fok, "Stretchable fiber-Bragg-grating-based sensor," *Optics Letters*, vol. 43, no. 11, pp. 2503–2506, June 2018, doi: 10.1364/OL.43.002503.

[16] E. S. L. Filho, M. D. Baiad, M. Gagné, and R. Kashyap, "Fiber Bragg gratings for low-temperature measurement," *Optics Express*, vol. 22, no. 22, p. 27681–27694, Oct. 2014, doi: 10.1364/OE.22.027681.

[17] Y. C. Chen, C. C. Hsieh, and C. C. Lin, "Strain measurement for composite tubes using embedded, fiber Bragg grating sensor, " *Sensors and Actuators A: Physical*, vol. 167, no. 1, pp. 63–69, May 2011, doi: 10.1016/j.sna.2011.02.035.

[18] N. Tanaka, Y. Okabe, and N. Takeda, "Temperature-compensated strain measurements using FBG sensors embedded in composite laminates, " *Proc. of SPIE, 9th International Symposium on Smart Structures and Materials 2002: Smart Sensor Technology and Measurement Systems*, vol. 4694, no. 7, pp. 304–313, July 2002, doi: 10.1117/12.472634.

[19] O. Almubaied, H. K. Chai, M. R. Islam, K. S. Lim, and C. G. Tan, "Monitoring corrosion process of reinforced concrete structure using FBG strain sensor, " *IEEE Transactions on Instrumentation and Measurement*, vol. 66, no. 8, pp. 2148–2155, Apr. 2017, doi:10.1109/tim.2017.2676218.

[20] J. Mao, J. Chen, L. Cui, W. Jin, C. Xu, and Y. He, "Monitoring the corrosion process of reinforced concrete using BOTDA and FBG sensors," *Sensors*, vol. 15, no. 4, pp. 8866–8883, Apr. 2015, doi:10.3390/s150408866.

[21] C. Hong, Y. Zhang, Z. Lu, and Z. Yin, "A FBG tilt sensor fabricated using 3D printing technique for monitoring ground movement," *IEEE Sensors Journal*, vol. 19, no. 15, pp. 6392–6399, Aug. 2019, doi: 10.1109/JSEN.2019.2908873

[22] S. F. Jiang, Z. H. Qiao, N. L. Li, J. Luo, S. Shen, M. H. Wu, and Y. Zhang, "Structural health monitoring system based on FBG sensing technique for Chinese ancient timber buildings," *Journal of Sensors*, vol. 20, no. 1, pp. 1–17, Dec. 2019, doi: 10.3390/s20010110.

[23] C. Tavares, C. Leitao, D. Lo Presti, M. F. Domingues, N. Alberto, H. Silva, and P. Antunes, "Respiratory and heart rate monitoring using an FBG 3D-printed wearable system," *Biomedical Optics Express*, vol. 13, no. 4, pp. 2299–2311, Apr. 2022, doi: 10.1364/boe.452115.

[24] L. Schenato, Q. Rong, Z. Shao, X. Quiao, A. Pasuto, A. Galtarossa, and L. Palmieri, "Highly sensitive FBG pressure sensor based on a 3D-printed transducer," *Journal of Lightwave Technology*, vol. 37, no. 18, pp. 4784–4790, Sep. 2019, doi: 10.1109/JLT.2019.2919917.

[25] M. G. Zubel, K. Sugden, D. J. Webb, D. Sáez-Rodríguez, K. Nielsen, and O. Bang, "Embedding silica and polymer fibre Bragg gratings (FBG) in plastic 3D-printed sensing patches," *Proc. of SPIE, Photonics Europe 2016, Micro-Structured and Specialty Optical Fibres IV*, vol. 9886, pp. 1–12, Apr. 2016, doi: 10.1117/12.2228753.

[26] C. Hong, Y. Zhang, and L. Borana, "Design, fabrication and testing of a 3D printed FBG pressure sensor," *IEEE Access*, vol. 7, pp. 38577–38583, Mar. 2019, doi: 10.1109/ACCESS.2019.2905349.

[27] N. N. Ismail, A.S. Sharbirin, M.S.M. Sa'ad, M.K.A Zaini, M.F. Ismail, G. Brambilla, B.M.A. Rahman, K.T.V. Grattan, and H. Ahmad, "Novel 3D-printed biaxial tilt sensor based on fiber Bragg grating sensing approach," *Sensors and Actuators A: Physical*, vol. 330, no. 112864, pp. 1–8, Oct. 2021, doi: 10.1016/j.sna.2021.112864.

[28] M. A. Alias, H. Ahmad, M. Z. Samion, M. S. M. Sa'ad, K. S. Lim, K. T. V. Grattan, B. M. A. Rahman, G. Brambilla, M. K. A. Zaini, L. Bayang, and M. F. Ismail, "Highly sensitive temperature-independent FBG-based sensor embedded in thermoplastic polyurethane using 3D printing technology for the measurements of torsion," *Sensors and Actuators A: Physical*, vol. 346, no. 113889, pp. 1–13, Oct. 2022, doi: 10.1016/j.sna.2022.113889.

[29] "PolyFlex™ PLA" Polymaker, https://polymaker.com/product/polymax-pla/ (accessed Nov. 2, 2022).

[30] "Filament Properties Table," Simplify3D, https://www.simplify3d.com/resources/materials-guide/properties-table/ (accessed Nov. 2, 2022).

[31] "PolyFlex™ TPU95," Polymaker, https://polymaker.com/product/polyflex-tpu95/ (accessed Nov. 2, 2022).

[32] "PolyMax™ PC" Polymaker, https://polymaker.com/product/polymax-pc/ (accessed Nov. 2, 2022).

[33] "PolyLite™ ABS" Polymaker, https://polymaker.com/product/polylite-abs/ (accessed Nov. 2, 2022).

[34] "PolyMax™ CoPa" Polymaker, https://polymaker.com/product/polymide-copa/ (accessed Nov. 2, 2022).

[35] S. P. Ugale and V. Mishra, “Modeling and characterization of fiber Bragg grating for maximum reflectivity,” *Optik*, vol. 122, no. 22, pp. 1990–1993, Nov. 2011. doi:10.1016/j.ijleo.2010.12.017.

[36] D. H. Kang, S. O. Park, C. S. Hong, and C. G. Kim, “The signal characteristics of reflected spectra of fiber Bragg grating sensors with strain gradients and grating lengths,” *NDT & E International*, vol. 38, no. 8, pp. 712–718, Dec. 2005. doi:10.1016/j.ndteint.2005.04.006.